TRAMAT 2 (2026) 100242

Contents lists available at ScienceDirect

Transactions of Materials Research

journal homepage: www.sciencedirect.com/journal/transactions-of-materials-research

Synergistic W-alloyed MoS_2 and Mo_2N barrier enable adaptive friction in MoAgN coatings under thermal cycling

Yong Cheng, Yupeng Zhang, Yingjie Wang, Yuxi Xu, Yiqun Feng, Zhenyu Wang *, Aiying Wang

State Key Laboratory of Advanced Marine Materials, Ningbo Institute of Materials Technology and Engineering, Chinese Academy of Sciences, Ningbo, 315201, China

ARTICLE INFO

Keywords:
Operando friction
Wide temperature range
Adaptive lubrication
MoN coating

ABSTRACT

Reliable low-friction, wear-resistant coatings that remain effective from room temperature to several hundred degrees are crucial for components such as foil air bearings, yet are difficult to realize because the dominant lubrication mechanism changes with temperature. Here we engineer a family of dual-layer MoAgN/MoS_2-W composite coatings in which Ag diffusion and solid lubrication are jointly controlled by a W-alloyed MoS_2 top layer and a columnar Mo_2N diffusion barrier. Under operando continuous-heating tests from 25 to 600 °C, the optimized coating containing a Mo_2N barrier (S3) sustains a friction coefficient below 0.4 across the entire temperature range and exhibits the lowest high-temperature friction (~0.23 at 600 °C). W alloying increases the hardness and elastic strain to failure of the MoS_2 top layer, enhancing its oxidation resistance and reducing the wear rate without compromising lubricity. Compared with the barrier-free MoAgN/MoS_2-W coating, the wear rate of S3 at 600 °C is reduced by a factor of 3.6. By combining micro-area XRD, Raman spectroscopy, SEM/EDS, and TEM, we resolve the temperature-dependent evolution of the tribofilm. Lubrication transitions from basal-plane MoS_2 shear at low temperature, to a self-organized "sandwich" tribofilm composed of a WO_3 base layer, an intermediate Ag reservoir, and a MoO_3/$AgTM_xO_y$ top layer at intermediate temperature, and finally to a liquid-like silver molybdate film coexisting with Mo oxides at 600 °C. High-low temperature cycling tests (RT-350 °C-RT-500 °C-600 °C-RT) show that S3 maintains reproducible low friction up to 500 °C, while exposure to 600 °C eventually pulverizes the oxide-based tribofilm and increases friction upon cooling. These results establish a materials and architecture-based design strategy for wide-temperature, self-adaptive solid-lubricant coatings, and provide mechanistic guidelines for managing noble-metal diffusion and tribochemical film formation in severe tribological environments.

1. Introduction

High friction and wear between moving pairs over a broad temperature range (particularly 25- 600 °C) severely limit the service life and operational reliability of components such as air foil bearings. Applying adaptive solid-lubricant coatings by physical vapor deposition (PVD) has emerged as an effective strategy, especially when combined with multiphase compounding and in situ formation of lubricating phases under service conditions [1] [2]. Transition metal nitride (TMN), particularly MoN-based systems, are attractive owing to their high hardness, wear resistance, and potential self-lubricating behavior via in situ formation of Magnéli-type MoO_3 during sliding [3] [4]. The easy-shear (101) planes of MoO_3 facilitate low friction at elevated temperatures [5] [6] [7]. However, MoO_3 becomes highly volatile above ~500 °C [8]. This volatilization leads to rapid depletion of the lubricating oxide phase from the sliding interface, directly compromising tribofilm stability by disrupting the formation of a continuous, load-bearing lubricious layer.

More critically, the continuous escape of MoO_3 vapor generates pores and voids within the coating matrix, progressively rendering the structure loose and porous. This volatilization-induced loosening weakens the mechanical integrity of the coating, promotes crack initiation and propagation, and ultimately leads to structural collapse and catastrophic failure of the protective layer. To overcome this limitation, soft metals with low shear strength such as Cu, Ag, and Au have been incorporated into TMN coatings to reduce the friction coefficient (COF) and enhance lubricity [9] [10] [11]. Among them, Ag is particularly appealing due to its high diffusion coefficient and tendency to segregate

* Corresponding author.
E-mail address: wangzy@nimte.ac.cn (Z. Wang).

https://doi.org/10.1016/j.tramat.2026.100242
Received 4 February 2026; Received in revised form 17 March 2026; Accepted 21 March 2026
Available online 23 March 2026

to the surface where it forms a lubricating film. In Ag-containing nitride coating systems, the adaptive lubrication behavior is dictated by two critical and interdependent processes: the temperature-activated diffusion of Ag and the dynamics of surface oxidation. At comparatively low temperatures (typically below 400 °C), Ag atoms migrate rapidly along microstructural imperfections, particularly columnar grain boundaries, toward the wear track. This migration promotes the establishment of a soft metallic lubricious layer, which effectively reduces the COF [12] [13]. As the temperature increases into the medium-to-high range (400-700 °C), the oxidation resistance of the coating becomes increasingly important. In systems such as MoN-Ag, however, oxidation does not necessarily lead to degradation but instead contributes constructively to adaptive lubrication. Previous investigations have demonstrated that layered ternary oxides, including Ag_2MoO_4 and $Ag_2Mo_4O_{13}$ [14] [15] [16], which form through reactions between Ag and transition metals such as Mo or V [17], exhibit intrinsically favorable lubricating characteristics. The overall oxidation behavior: governed by the competing kinetics of oxide nucleation, growth, and Ag diffusion-ultimately dictates the durability and stability of the coating under elevated-temperature service conditions.

Extensive studies have been devoted to Ag-doped TMN coatings in recent years [18] [19]. However, these coatings also highlight a fundamental trade-off: the very high Ag diffusivity that benefits lubrication at early stages also drives rapid Ag depletion under sustained sliding, leaving behind a porous, mechanically weakened matrix and limiting long-term performance. Moreover, most existing studies focus on coating structure and tribological properties at constant temperatures, providing limited insight into sustained friction behavior under varying temperatures, which does not adequately reflect real operating conditions.

In parallel, layered dichalcogenides such as MoS_2 and WS_2 are classical solid lubricants with very low shear strength, but they are inherently soft (1.5-5 GPa) and susceptible to wear, which restricts their use as standalone protective coatings [20] [21]. Alloying MoS_2 with W has been shown to enhance hardness and oxidation resistance, and the Magnéli-type oxide WO_3 formed at high temperature contributes additional load-bearing capacity and lubrication [22] [23] [24]. Ma et al. [25] demonstrated that MoS_2/Ag composite films exhibit lower wear rates than pure MoS_2 in both vacuum and air because ductile Ag fills defects and pores in the sliding interface, forming a denser tribofilm and a smoother sliding contact.

Holmberg and Matthews proposed a structural design concept in which a relatively soft, lubricious top layer is supported by a hard underlayer that provides mechanical support and wear resistance [26]. Building on this concept, an ideal wide-temperature adaptive coating would integrate: (i) a hard, Ag-containing nitride base that can supply Ag and withstand high contact stresses; (ii) a mechanically robust, oxidation-resistant dichalcogenide-based top layer that preserves low friction at lower temperatures; and (iii) an internal diffusion barrier that moderates Ag transport, avoiding both premature depletion and structural destabilization.

Here we implement this strategy in a family of MoAgN/MoS_2-W dual-layer coatings. The coatings consist of a MoAgN bottom layer, a W-alloyed MoS_2 top layer, and, in the optimized design, a dense columnar Mo_2N diffusion barrier embedded in the MoAgN layer. The operando tribological properties and microstructural evolution of the coating over a wide temperature range were systematically investigated, and the underlying anti-friction and failure mechanisms at different temperatures are discussed in detail.

2. Experiment

2.1. Coating deposition

Ni-based superalloy, high-speed steel and Si wafers were used as substrates for tribological and microstructural characterization, respectively. Before deposition, substrates were ultrasonically cleaned in acetone and anhydrous ethanol for 15 min each, dried, and mounted on a rotating holder using conductive clips. The deposition chamber was evacuated to a base pressure of 3.0×10^{-5} Pa. To remove native oxides and adsorbed contaminants, the substrate surfaces were etched for 45 min using a linear anode-layer ion beam. The etching parameters were: Ar flow 45 mL/min, ion source current 0.2 A, acceleration voltage 1200 V, and substrate bias −200 V.

The MoAgN/MoS_2-W coating with columnar Mo_2N diffusion barrier layer (named S3) was subsequently fabricated beginning with the deposition of a Mo transition layer for 20 min, resulting in a thickness of approximately 200 nm. To improve coating adhesion, a Mo_2N transition layer was then deposited. This was followed by the deposition of a MoAgN layer incorporating an intermediate columnar-structured Mo_2N interlayer. Specifically, the MoAgN layer was deposited for 150 min, after which the N_2 gas and Ag target were switched off to deposit a pure Mo_2N layer for 15 min. The N_2 and Ag target were then resumed to continue MoAgN deposition for another 150 min. Before fabricating the top MoS_2-W layer, replace the Mo target and Ag target with MoS_2 target and W target, and perform etching treatment on the surface of the fabricated coating. Then, a W transition layer was applied for 5 min (~90 nm thick) to enhance interlayer adhesion. The MoS_2-W composite layer was subsequently co-deposited using DC power supplies connected to both MoS_2 and W targets for 45 min. The specific deposition parameters are shown in Table 1.

The MoAgN/MoS_2-W coating without columnar Mo_2N diffusion barrier layer (named S2) was deposited in the same manner as S3 but without the insertion of the Mo_2N interlayer in the MoAgN layer. The MoAgN/MoS_2-W coating with columnar Mo_2N diffusion barrier layer (named S1), differed by having the W target deactivated during the deposition of the top layer, which was instead a pure MoS_2 film deposited for an additional 5 min. The schematic diagram of the coating deposition is shown in Fig. 1.

2.2. Microstructural characterizations

Phase composition of the coatings deposited on high-speed steel was characterized by X-ray diffraction (XRD, Bruker AXS D8 Advance, Germany) over 20-80°, using Cu Kα radiation. Microstructures were examined by field-emission scanning electron microscopy (FE-SEM, Verios G4 UC) on coatings deposited on Si. Additionally, a Quanta 250 FEG SEM, integrated with an energy-dispersive X-ray spectroscopy (EDS) detector, was employed to observe surface morphology, chemical composition, and worn surfaces generated during tribological tests on nickel-based superalloy substrates. The SEM was operated at an accelerating voltage of 15 kV. Mechanical properties, including hardness (H) and elastic modulus (E), were evaluated using a Nano Indenter G200 system equipped with a Berkovich diamond tip (apex angle 70.32°, tip radius 30 nm). The continuous stiffness measurement (CSM) technique was applied, with the maximum penetration depth restricted to 10 % of the total coating thickness to reduce substrate influence. The tests were conducted at a loading strain rate of 0.05 s^{-1} and an unloading rate of 4 mN/s. Nanoindentation measurements were performed with a minimum of 8 indents on each sample to obtain statistically reliable values. To investigate phase evolution following friction tests, micro-area XRD analysis was carried out using a VANTEC500 system with a 2D detector (spot size: 0.5 mm^2). Complementary phase identification was performed via confocal Raman spectroscopy (Renishaw) with a 532 nm laser. Raman mappings were taken from three distinct regions to verify reproducibility. Microstructural analysis was further conducted by transmission electron microscopy (TEM) on a Talos F200X instrument operating at 200 kV. TEM samples were prepared through focused ion beam (FIB) milling using a Carl Zeiss Auriga dual-beam system.

Table 1
Deposition parameters of S3 coating.

	Bias Voltage (V)	Mo Target (HiPIMS)			Ag Target (DCMS) Power (W)	MoS_2 Target (DCMS) Power (W)	W Target (DCMS) Power (W)	Ar Flow (sccm)	N_2 Flow (sccm)	Deposition Time (min)
		Duty ratio (%)	Frequency (kHz)	Power (W)						
Mo Transition Layer	−200	5	1	1500	-	-	-	50	0	20
Mo_2N Transition Layer	−150	2.5	0.5	1700	-	-	-	50	60	15
MoAgN Layer	−150	2.5	0.5	1700	100	-	-	50	60	300
Mo_2N barrier Layer	−150	2.5	0.5	1700	-	-	-	50	60	15
W Transition Layer -	−150	-	-	-	-	-	1000	50		5
MoS_2-W Layer	−150	-	-	-	-	1000	100	50	-	45

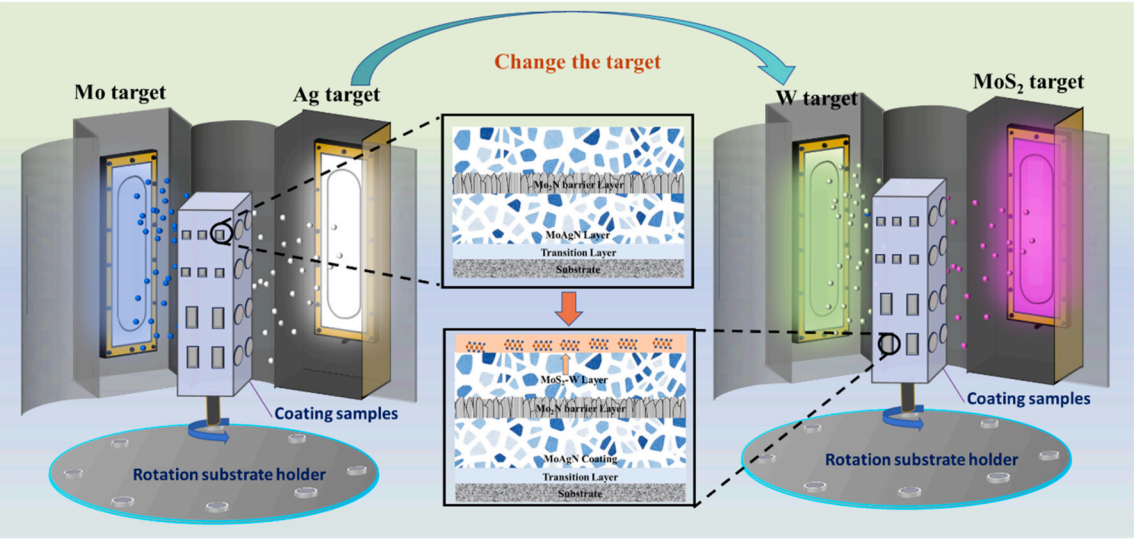

Fig. 1. Schematic diagram of the equipment.

2.3. Tribological tests

Tribological behavior was evaluated using a high-temperature ball-on-disk tribometer (Anton Paar, THT). To simulate realistic service conditions, an operando continuous-heating protocol was employed in which a single wear track was tested sequentially at 25, 350, 500, and 600 °C, without interrupting sliding between stages. For comparison, isothermal tests were also conducted at each temperature on fresh tracks. A φ 6 mm Al_2O_3 ball was used as the counterbody. The normal load was fixed at 2 N, corresponding to a Hertzian contact pressure of 982.6-1129.8 MPa over the temperature range. The sliding speed was 5 cm/s, the wear-track radius was 5 mm, and the sliding distance was 25 m per stage. All tribological tests were repeated three times (N = 3) under identical conditions to ensure reproducibility.

The wear rate (W_R) was determined using the following formula [27] [28]:

$$W_R = \frac{S \times l}{N \times L} \quad (1)$$

where S represents the cross-sectional area of the wear track (mm^2); l denotes the track length (mm); N is the applied load (N); L is the total sliding distance (m).

3. Results and discussion

3.1. Layer architecture and mechanical properties

Cross-sectional SEM images (Fig. 2a–c) reveal sharp and well-defined interfaces between the coatings and the Ni-based superalloy substrate, indicative of good adhesion. From top to bottom, the architecture consists of a MoS_2-W lubricating layer (~1.2 μm), a W transition layer (~80-90 nm), a MoAgN bottom layer incorporating a columnar Mo_2N diffusion barrier (in S3), and a Mo_2N/Mo bilayer directly on the substrate. The total coating thickness is about 5.0-5.5 μm. In S3, the Mo_2N barrier interrupts the continuous columnar growth in the MoAgN layer and is expected to slow Ag transport along column boundaries. EDS analysis shows that the S/Mo atomic ratio in the MoS_2-W top layer is close to the nominal 2:1. Slight deviations can be attributed to the higher sputtering yield of S under Ar^+ bombardment and to secondary reactions consuming S through interaction with residual O, N, and H_2O in the chamber [29].

XRD patterns of the as-deposited coatings (Fig. 3a) indicate a composite structure comprising face-centered cubic Mo_2N (ICDD 25-1366), crystalline W (ICDD 04-0806), MoS_2 (ICDD 37-1492), and metallic Ag (ICDD 04-0783). For S2 and S3, only the (002) reflection of MoS_2 is observed, demonstrating strong (002) texture. Previous work has shown that W additions suppress nucleation on prismatic (100) planes while promoting growth along the basal (002) planes, consistent with a rearrangement of the MoS_2 structure that favors expansion along the basal direction [30]. Because different MoS_2 planes exhibit distinct

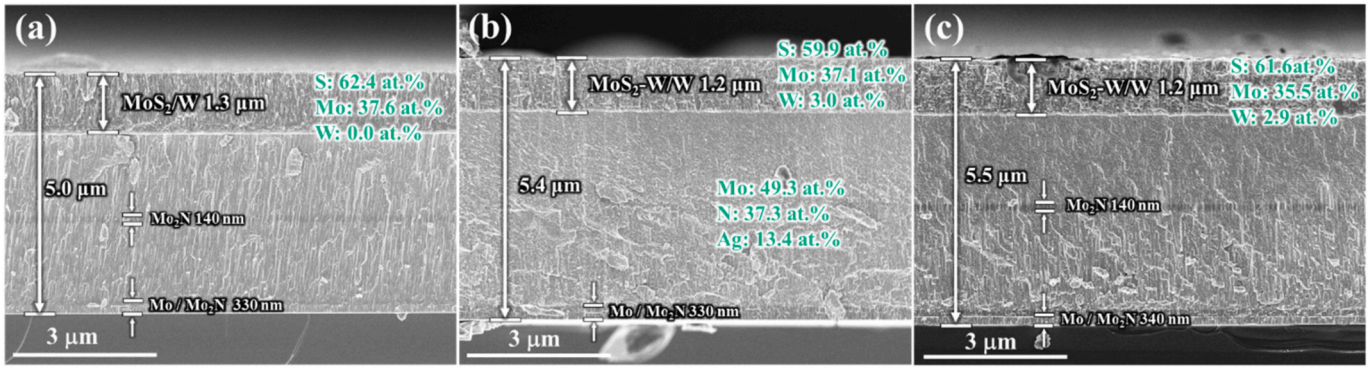

Fig. 2. Cross-sectional morphologies of different coatings, (a) S1; (b) S2; (c) S3.

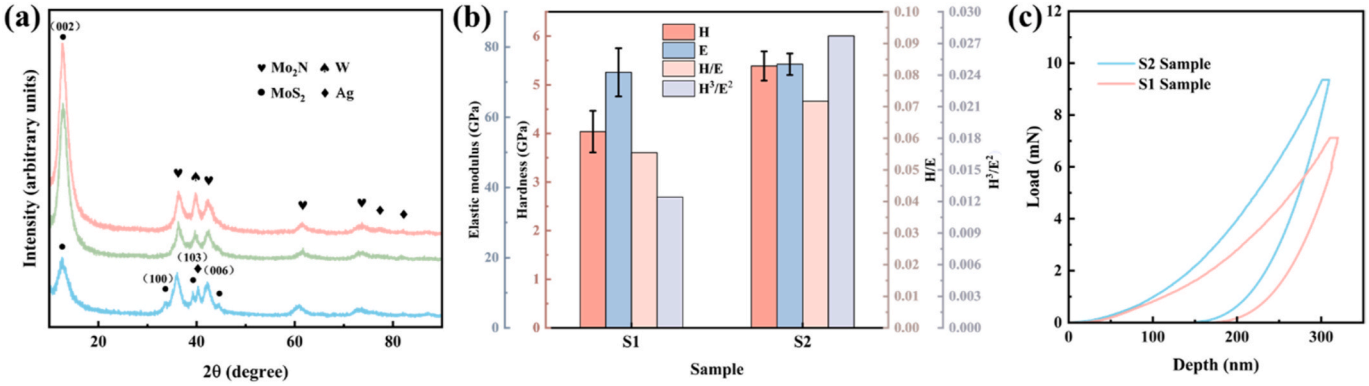

Fig. 3. (a) XRD of deposited coatings; (b) mechanical properties and (c) load-displacement curves of S2 and S1 samples.

tribological behaviors, this texture is important: basal planes allow easy interlayer shear and low friction, whereas prismatic planes oxidize more readily and hinder lubrication [31]. W alloying therefore simultaneously improves oxidation resistance and enhances frictional performance by stabilizing basal-plane oriented MoS_2.

Nanoindentation results for the MoS_2 and MoS_2-W top layers (S1 and S2) are summarized in Fig. 3b. The hardness increases from 4.0 GPa for pure MoS_2 to 5.4 GPa for MoS_2-W. Load-displacement curves of S1and S2 coatings are presented in Fig. 3c. All samples display smooth curves without discontinuities, indicating a low density of internal defects and a relatively dense, uniform coating structure. S2 coating require higher loads to reach the same indentation depth, further confirming that W alloying can enhance the mechanical properties of MoS_2 coatings, consistent with the increase in hardness. The increase in H/E upon W alloying signifies a higher elastic strain to failure, which is directly correlated with improved wear resistance in tribological contacts. Similarly, the enhanced H^3/E^2 ratio suggests a greater resistance to plastic deformation, a parameter strongly linked to the durability of coatings under repeated sliding contact [32] [33]. These improvements in mechanical integrity are consistent with the superior wear performance observed for S2 and S3 compared to S1, particularly at elevated temperatures (Fig. 4) where plastic deformation and cracking are more likely to occur.

3.2. Operando tribology under continuous heating

3.2.1. Friction coefficient and wear rate

The friction curves of S1-S3 during continuous heating from 25 to 600 °C are shown in Fig. 4a–c. At RT and 350 °C, all three coatings exhibit low and stable COFs of about 0.08. At 500 °C, the coatings begin to diverge: S3 maintains a COF of ~0.1 for an extended period before gradually increasing to ~0.4 after ~1300 s, whereas S2 shows a monotonic increase with strong fluctuations and S1 exhibits a sharp jump to ~0.6. At 600 °C, S3 displays the lowest steady-state COF (~0.23), outperforming S1 (~0.38) and S2 (~0.30).

The wear rate as a function of temperature is plotted in Fig. 4d. W_R increases with temperature for all coatings, but the magnitude and rate of increase differ. At RT and 350 °C, S2 and S3 exhibit similar, relatively low W_R values. By contrast, S1 shows a larger W_R, consistent with its wider and deeper wear tracks (Fig. 4f, f1), highlighting the beneficial effect of W alloying in the MoS_2-W top layer. At 600 °C, the W_R of S2 rises sharply to 5.6×10^{-4} mm^3 N^{-1} m^{-1}, which is 3.6 times higher than that of S3.

Surface images after the RT-500 °C stages (Fig. 4e) reveal that S2 is covered with large, coalesced Ag particles, indicative of extensive Ag diffusion and aggregation at high temperature. In contrast, S3 exhibits fewer and smaller Ag particles, demonstrating that the Mo_2N barrier effectively moderates Ag transport. Because Ag diffuses rapidly and is continuously consumed by wear and oxidation, uncontrolled Ag outdiffusion leaves behind a porous, mechanically weakened matrix that fails prematurely. By limiting Ag flux, the Mo_2N barrier in S3 delays this degradation and sustains a more optimal balance between lubrication and structural stability. Similar diffusion barriers in TMN matrices have been shown to effectively suppress noble-metal transport [34]. Overall, these operando tests show that the combination of W-alloyed MoS_2-W and a Mo_2N diffusion barrier is essential for achieving both low friction and low wear over the full 25-600 °C window.

3.2.2. Phase evolution and tribofilm chemistry

To elucidate the origin of the distinct friction regimes, we performed micro-area XRD and Raman spectroscopy on the wear tracks of S3 after each temperature stage (Fig. 5). At RT and 350 °C, micro-area XRD patterns (Fig. 5a) closely resemble those of the as-deposited coating, indicating that the bulk structure remains largely unchanged. Raman

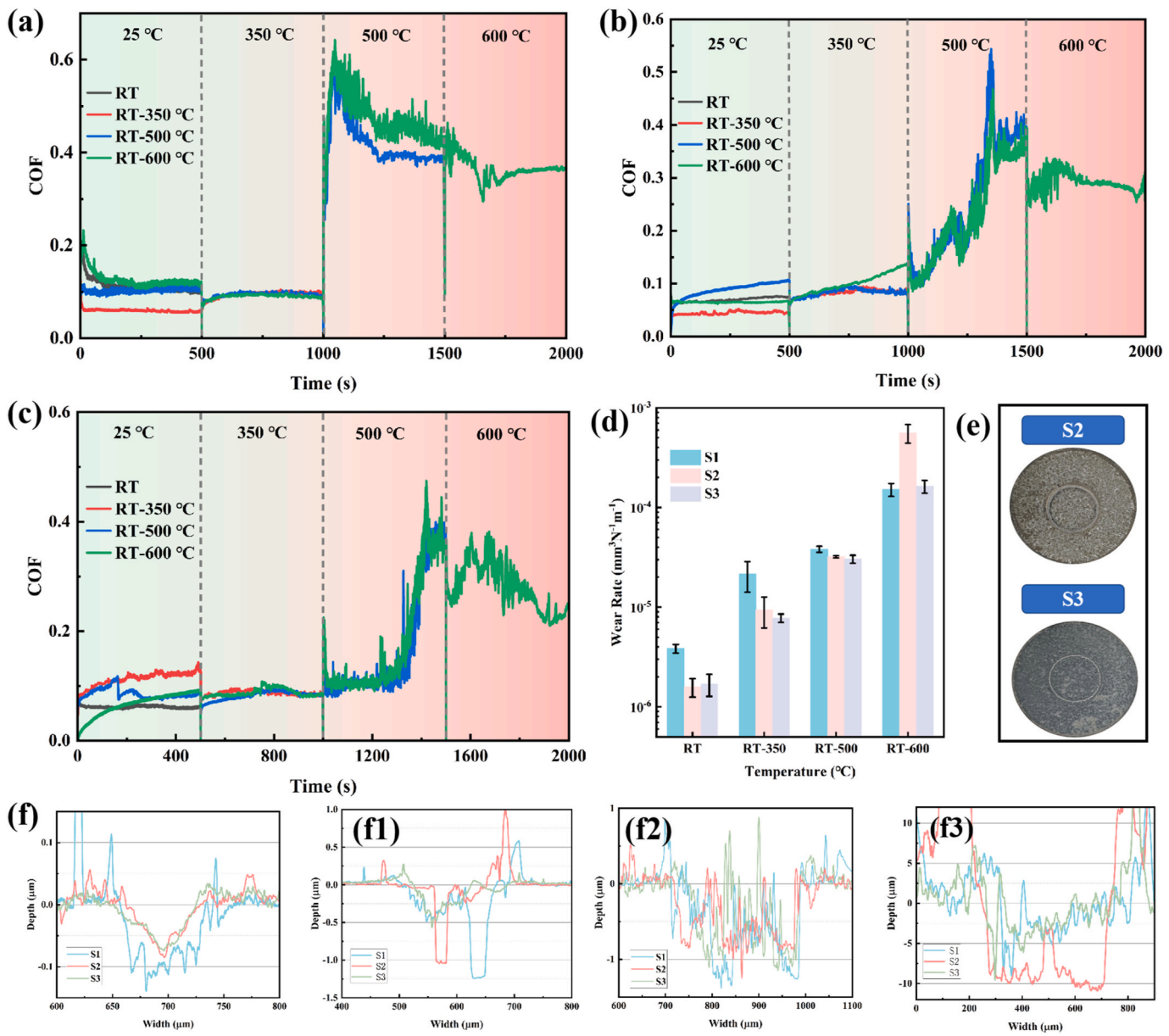

Fig. 4. The friction curves of S1 (a), S2 (b), S3 (c) and corresponding W_R (d); Surface morphology of samples after friction at the RT-500 °C stage (e); Two-dimensional microstructure of wear tracks: RT (f), RT-350 °C (f1), RT-500 °C (f2), RT-600 °C (f3) during continuous heating friction tests of the three samples.

spectra (Fig. 5b) show characteristic MoS_2 peaks at ~379, 418, 525, and 656 cm^{-1} [35] [36], together with weak signals from MoO_3 and MoO_2, consistent with mild tribo-oxidation confined to the near-surface region. In this regime, lubrication is dominated by interlayer shear within the basal-plane oriented MoS_2-W top layer.

At 500 °C, the Raman signatures of MoS_2 disappear and are replaced by strong peaks associated with WO_3, MoO_3, $AgTM_xO_y$ (e.g., $Ag_2Mo_4O_{13}$), and metallic Ag. Magnéli-type WO_3 and MoO_3 possess crystallographic shear planes that promote sliding, and they are thermally stable, exhibit relatively low tribo-oxidation susceptibility, and display modest interfacial adhesion [37] [38]. $AgTM_xO_y$ have layered structures with relatively weak Ag-O bonds. Under shear, fracture preferentially occurs along Ag-O rather than TM-O bonds, enabling easy interlayer slip. Together with soft FCC Ag, which has a low critical shear stress (~0.588 MPa) [39], these phases form a mixed oxide-metal tribofilm that maintains low COF at intermediate temperatures.

At 600 °C, oxidation is more extensive, and the tribofilm becomes richer in complex metal and bimetallic oxides. In particular, $AgTM_xO_y$ such as Ag_2MoO_4 and $Ag_2Mo_4O_{13}$ have reported melting points of approximately 560 °C and 574 °C, respectively. These values lie just below our test temperature of 600 °C, indicating that these phases are expected to be at least partially molten under the sliding conditions employed [40]. As discussed below, this melting produces a liquid-like film that plays a central role in high-temperature lubrication.

3.2.3. *Wear-track morphology and transfer films*

SEM images of the S3 wear track at different stages (Fig. 6a–d) reveal the evolution of wear mechanisms. At RT (Fig. 6a), the wear track is smooth with limited debris along the edges, indicating mild abrasive wear and a low W_R. After sliding at RT-350 °C (Fig. 6b, b1), the track becomes more porous and contains more debris, reflecting increased material removal. High-magnification images show grooves, cracks, and local fracture, consistent with more severe abrasion. EDS confirms that friction is still confined to the MoS_2-W layer, and an oxygen content of ~10.0 at.% indicates moderate oxidation. Despite this, the COF remains comparable to that at RT because the reduction in humidity at 350 °C

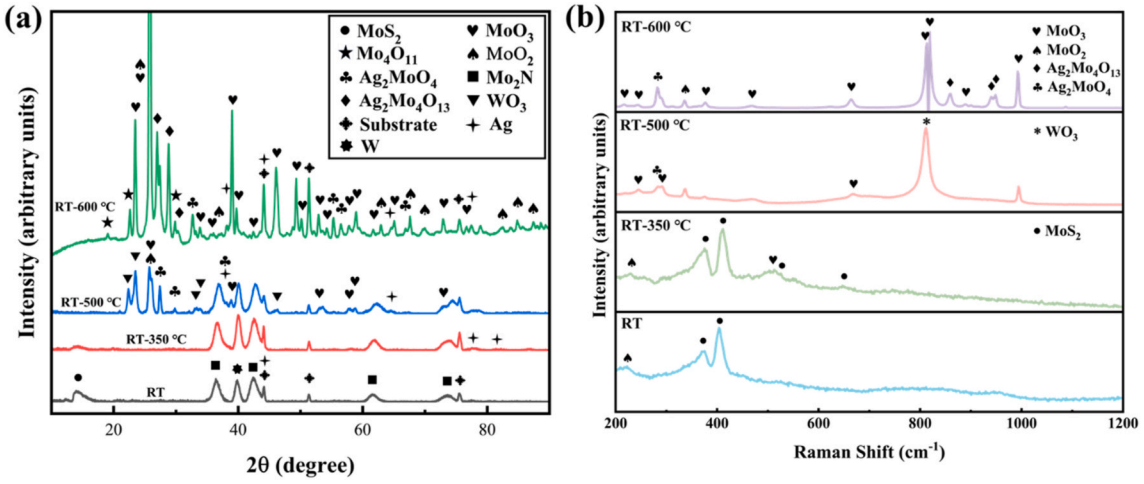

Fig. 5. The micro-area XRD patterns (a); Raman patterns (b) at the wear track after continuous heating friction of S3 sample.

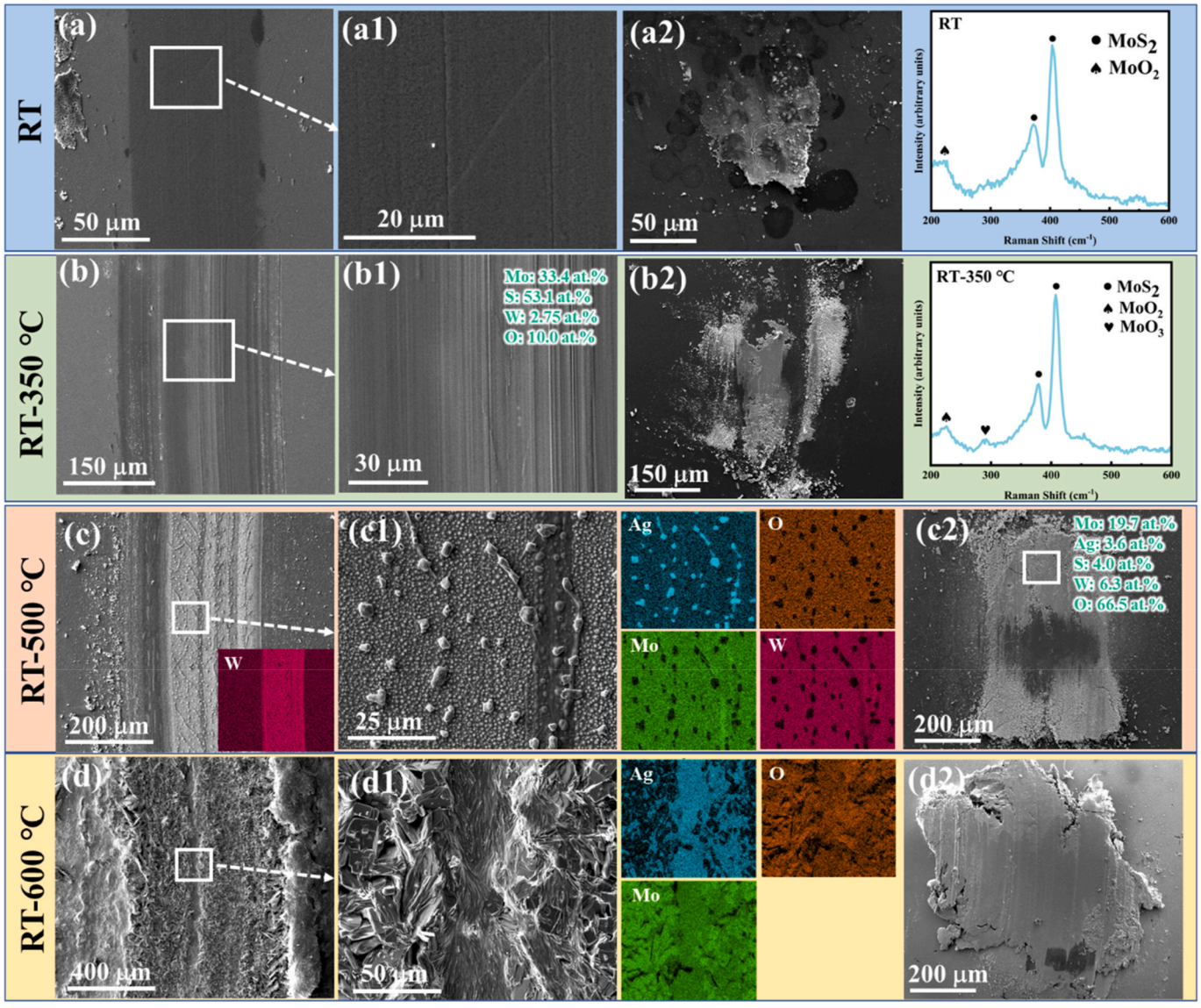

Fig. 6. The morphology of counterpart ball surface, wear track and elemental distribution of RT(a, a1,a2); RT-350 °C(b, b1,b2); RT-500 °C(c, c1,c2); RT-600 °C(d, d1,d2) after continuous heating friction of S3 sample.

offsets the detrimental effect of water adsorption on MoS_2 lubrication at RT [41] [42]. On the Al_2O_3 ball (Fig. 6a2, b2), a smooth transfer film forms after the first two stages, with no pronounced ploughing marks. Raman analysis shows that this film is dominated by MoS_2 with minor contributions from Mo oxides. The presence of a coherent transfer film on the ball and a continuous MoS_2-W layer on the coating together account for the stable, low COF in this temperature range.

After the RT-500 °C stage (Fig. 6c, c1), the wear-track interior is enriched in Ag, O, and W, consistent with the presence of WO_3, $AgTM_xO_y$, and residual Mo oxides inferred from XRD and Raman. Initially, the intact MoS_2-W top layer provides very low friction (COF ~0.1). As sliding proceeds, accelerated oxidation and decomposition of MoS_2 at 500 °C rapidly consume the top layer and expose the W transition layer, leading to a transient increase in COF before a new tribochemical steady state is reached. For S1, which lacks W in the MoS_2 layer, the poorer mechanical and oxidation resistance leads to faster removal of the top layer and sharper friction spikes. For S2, the absence of a diffusion barrier permits unrestrained Ag out-diffusion, destabilizing the MoS_2-W layer and causing strong COF fluctuations. At the end of the third stage (Fig. 6c2), the central contact region on the ball is largely devoid of transfer film, although coating residues and W-containing debris accumulate near the periphery. This marks a dynamic equilibrium where lubricating oxides and $AgTM_xO_y$ are continuously formed and worn away, yielding a stabilized COF.

At 600 °C (Fig. 6d, d1), the wear track widens and edge debris increases, reflecting coating softening and stronger adhesion under severe oxidation. The central load-bearing zone is rich in Ag, Mo, and O, consistent with the formation of $AgTM_xO_y$ and Mo oxides. Rectangular

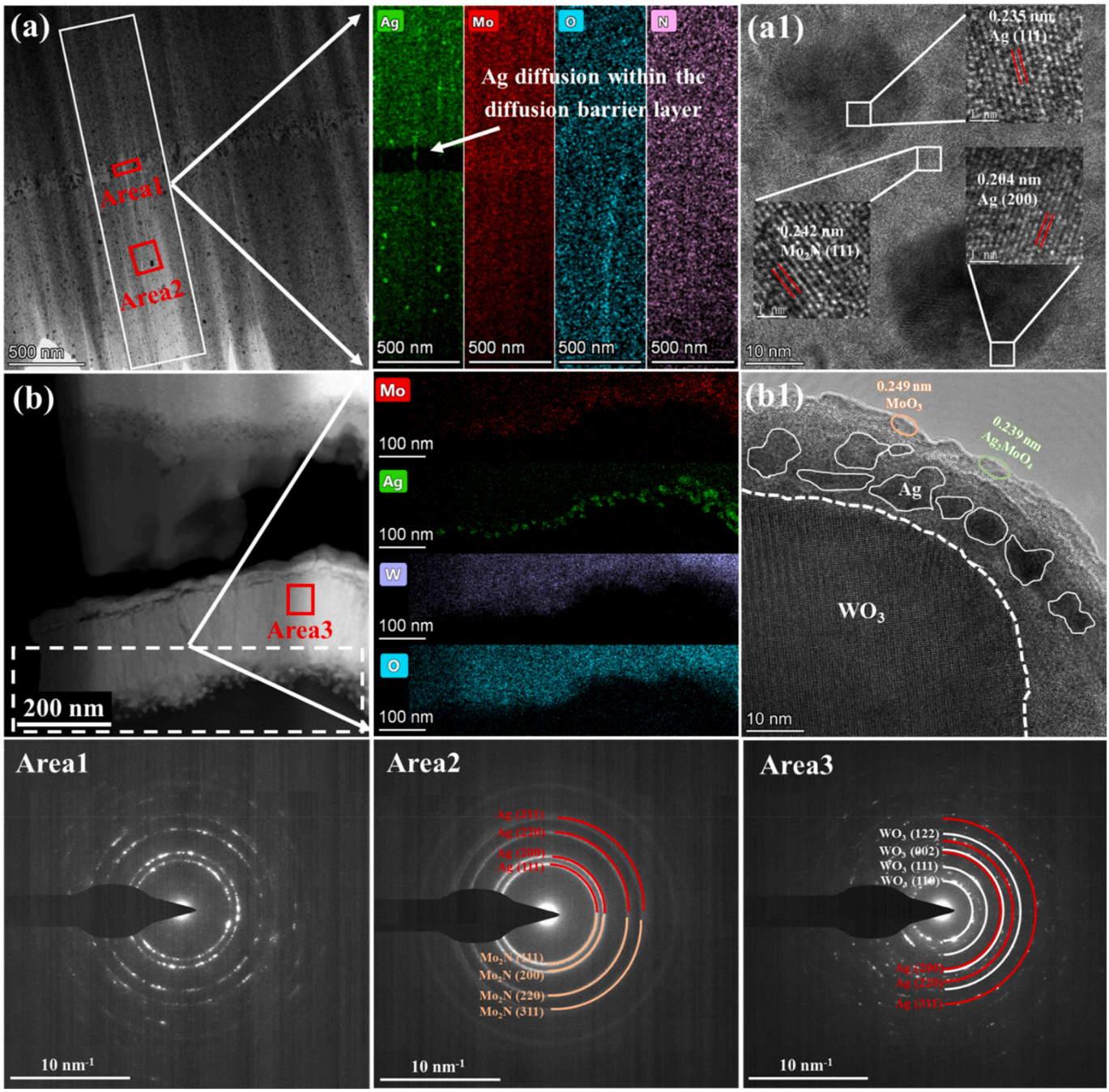

Fig. 7. (a),(b) Microstructure and EDS mapping; (a1),(b1) HRTEM images and three SAED patterns of S3 coating after continuous heating friction test at RT-500 °C.

Mo-oxide particles coexist with plastically deformed Ag-Mo-O compounds. Because $AgTM_xO_y$ with low melting points are partially molten, they form a semi-liquid film that fills the track and adheres to the ball. This film continuously renews as the molten material is transferred between the coating and the ball, and it is responsible for the relatively low COF (~0.23) observed at 600 °C. Fig. 6 reveal several features characteristic of molten or semi-liquid behavior: (i) The tribofilm exhibits smooth, flow-like features with rounded, elongated contours that suggest viscous flow under shear stress. These morphologies are distinctly different from the angular, faceted oxide particles observed at 500 °C (Fig. 6c1). (ii) Wear debris particles at 600 °C display rounded edges and smooth surfaces, in contrast to the sharp, irregular debris produced at lower temperatures. This rounding is consistent with partial melting and subsequent solidification upon cooling. (iii) The transfer film on the Al_2O_3 counterbody at 600 °C (Fig. 6d2) exhibits a smooth appearance: features characteristic of a low-viscosity liquid film that has been sheared and then solidified upon cooling.

3.2.4. *Diffusion-barrier function and subsurface structure*

TEM analysis of S3 after the RT-500 °C stage (Fig. 7a) shows that the MoAgN/Mo_2N stack beneath the tribofilm remains dense, with a well-preserved columnar nanocomposite structure. Ag clustering is observed on both sides of the Mo_2N barrier, indicating that Ag diffuses along columnar grain boundaries toward the surface but is partially impeded by the barrier. This confirms that the Mo_2N interlayer does not completely block Ag diffusion but slows it sufficiently to enable a controlled release that balances lubrication with structural integrity.

High-resolution TEM images (Fig. 7a1) reveal larger particles with lattice spacings of 0.204 and 0.235 nm, corresponding to Ag, surrounded by Mo_2N grains with a spacing of 0.241 nm. Together with EDS maps, these observations show that elevated temperatures promote Ag segregation to Mo_2N grain boundaries. As described by Ostwald ripening [43] [44] [45], Ag atoms diffuse from smaller to larger clusters, leading to coarsening. Initially, defects at grain boundaries can accommodate the growth of Ag particles; once these sites are saturated, further coarsening is constrained until a higher thermal driving force triggers macroscopic Ag migration to the surface [46].

Selected-area electron diffraction (SAED) patterns acquired from regions immediately at and above the Mo_2N barrier (inset in Fig. 7a) contain overlapping rings from c-Ag and γ-Mo_2N due to their similar lattice spacings. The broader, more intense Ag-related rings in the region above the barrier indicate a higher Ag concentration, demonstrating that most Ag accumulates on the barrier's upper side while only a limited fraction penetrates through.

TEM analysis of the friction layer (Fig. 7b, b1) reveals a stratified tribofilm consisting of a WO_3-rich layer adjacent to the coating, an intermediate Ag-rich zone, and a top layer containing MoO_3 and $AgTM_xO_y$. SAED patterns confirm the presence of WO_3 and Ag-bearing oxides in these regions. This structure corresponds to the "sandwich" tribofilm inferred from Raman and XRD. In this configuration, the Al_2O_3 ball first contacts WO_3 and surface Ag particles; Ag undergoes plastic deformation and spreads, while MoS_2-derived material from earlier stages is reincorporated into the wear track and reacts with Ag and Mo oxides to form $AgTM_xO_y$. Simultaneously, WO_3 is transferred to the ball, establishing a dynamic material exchange. The intermediate Ag layer acts as both a lubricant and a reservoir for ongoing silver molybdate formation. This self-organized tribofilm architecture is central to maintaining low friction and suppressed wear over the intermediate-temperature regime.

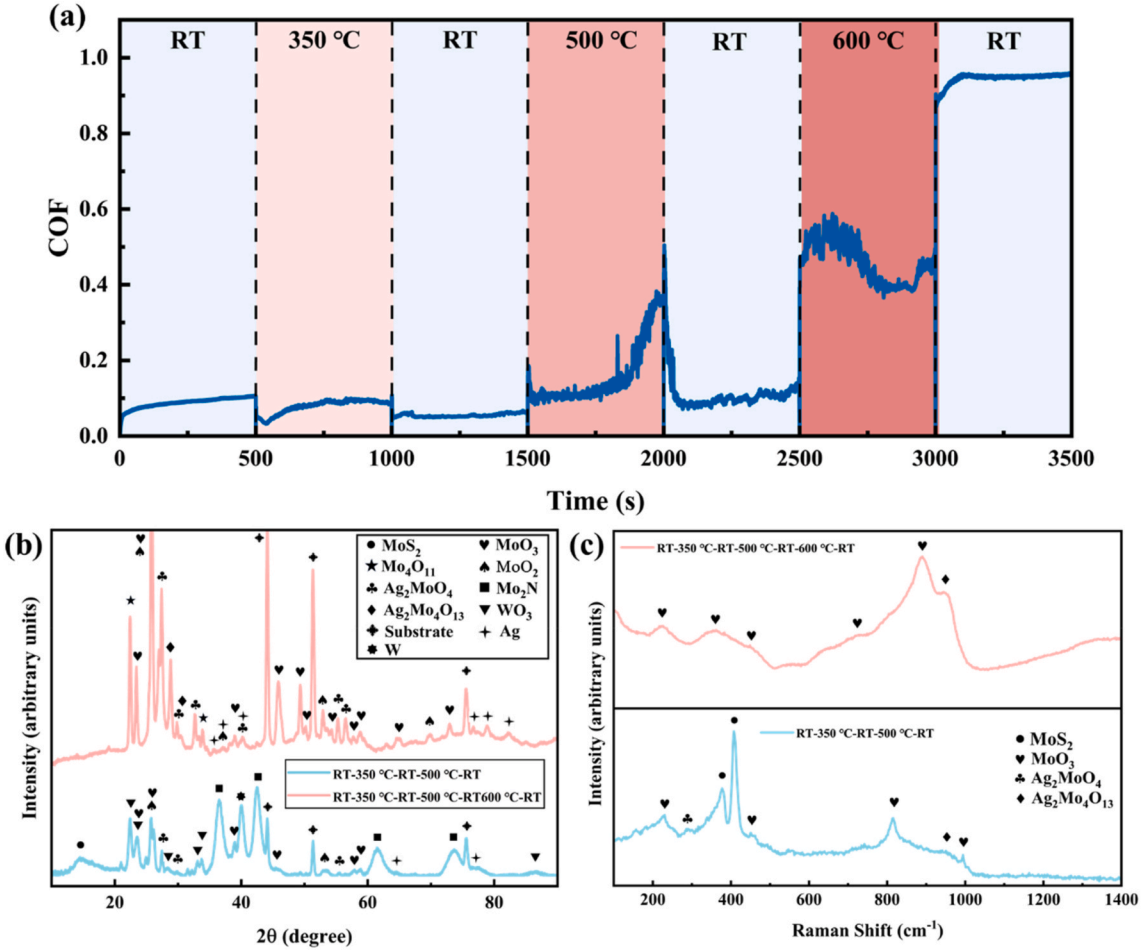

Fig. 8. The friction curves (a); micro-area XRD patterns (b) and Raman patterns (c) at the wear track after temperature-cycling friction tests of S3 sample.

3.3. High-low temperature cycling

To approximate service conditions involving repeated heating and cooling, high-low temperature cycling tests were conducted on S3. The friction curves and corresponding phase analyses are shown in Figs. 8 and 9.

During the RT-350 °C-RT sequence, the MoS_2-W top layer remains largely intact, and the COF stays below 0.1. When the temperature is raised to 500 °C, the COF initially remains around 0.1 but gradually increases to ~0.4 as oxidation and thinning of the MoS_2-W layer proceed. Upon subsequent cooling to RT on the same track, the COF stabilizes at ~0.12 after an initial running-in period. When the temperature is then increased to 600 °C, the COF first rises and then stabilizes between 0.4 and 0.45: higher than in the continuous-heating test-reflecting the fact that prior cycling has already consumed part of the lubricating reservoir. In the final RT stage, the COF increases markedly to ~0.95. Despite this eventual degradation, the coating exhibits generally stable and repeatable behavior up to 500 °C, indicating robust performance under moderate thermal cycling.

Micro-area XRD patterns collected after cycles up to 500 °C and 600 °C (Fig. 8b) show that, after RT-350 °C-RT-500 °C-RT, the wear track still contains both lubricating oxides ($AgTM_xO_y$, MoO_3, WO_3) and residual MoS_2. This contrasts with the continuous-heating case at 500 °C, in which MoS_2 is fully consumed (Fig. 5). Raman spectra (Fig. 8c) confirm the presence of MoS_2 in the cycled sample. Thus, under cycling up to 500 °C, the MoS_2-W top layer is only partially worn, and basal-plane MoS_2 shear remains a dominant lubrication mechanism. After a cycle including 600 °C, by contrast, MoS_2 is completely oxidized or removed, and the wear track becomes entirely composed of oxides and Ag-based lubricating phases.

SEM images of the wear tracks at intermediate and final cycling stages (Fig. 9) shed light on how these microstructural changes affect friction. After RT-350 °C-RT-500 °C (Fig. 9a, a1), the central load-bearing region is still covered by MoS_2-W, whereas peripheral regions have spalled, exposing the W transition layer. Within the MoS_2-W region, fine Ag particles and blister-like features are observed, indicating subsurface Ag accumulation and local delamination. The low initial COF (~0.1) at 500 °C is driven by a combination of MoS_2 shear and Ag-mediated lubrication. As sliding proceeds, severe oxidation, blistering, and partial spallation of the MoS_2-W layer roughen the surface and increase the COF to ~0.4.

Following an additional RT stage (Fig. 9b, b1), the track interior still contains MoS_2-W but appears smoother: Ag particles and blisters are gradually crushed and smeared by the counterbody, which explains why the COF decreases from ~0.45 to ~0.12 during this segment.

After completing the full RT-350 °C-RT-500 °C-RT-600 °C-RT cycle (Fig. 9c, c1), $AgTM_xO_y$ and Mo oxides are still generated at 600 °C but are extruded toward the edges as loose, powdery debris. The central region of the wear track is filled with a porous, incoherent oxide powder, rather than a compact, adherent tribofilm. The absence of a stable transfer film on the ball contact area (inset) indicates that lubrication no longer proceeds through a continuous solid or liquid film, but instead approaches dry sliding, accounting for the high COF (~0.95) in the final RT stage. These observations emphasize that maintaining a dense, mechanically robust tribofilm is essential for sustaining low friction under repeated thermal cycling.

3.4. Temperature-dependent lubrication mechanisms

Fig. 10 summarizes the temperature-dependent lubrication mechanisms of the S3 coating during continuous heating. At low temperature (RT-350 °C; Fig. 10a), the Al_2O_3 ball slides on the MoS_2-W top layer. A MoS_2-rich transfer film forms on the ball, and lubrication is dominated by interlayer sliding of basal-plane oriented MoS_2. Slight oxidation

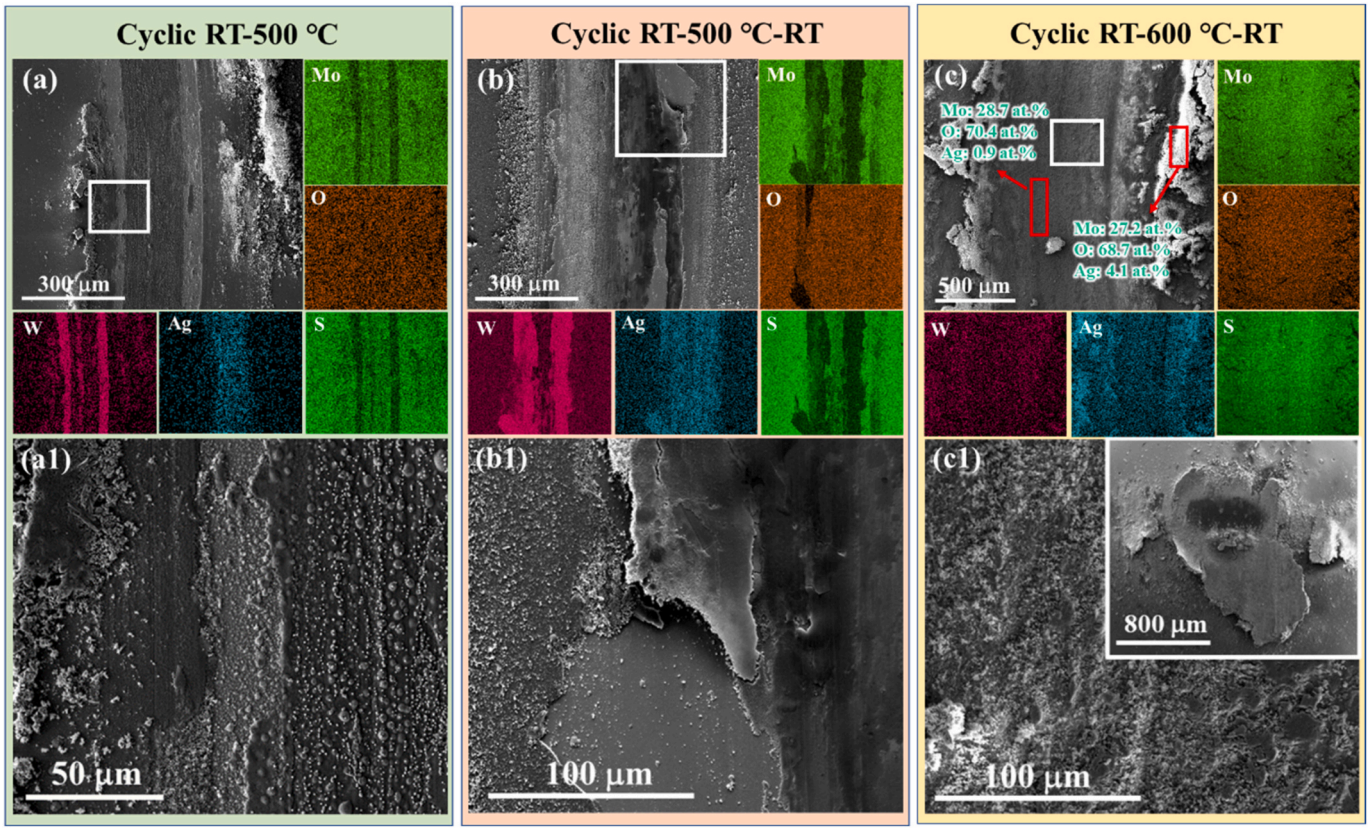

Fig. 9. The wear track and elemental distribution of RT-350 °C-RT-500 °C (a, a1); RT-350 °C-RT-500 °C-RT (b, b1); RT-350 °C-RT-500 °C-RT-600 °C-RT (c, c1); after temperature-cycling friction of S3 sample.

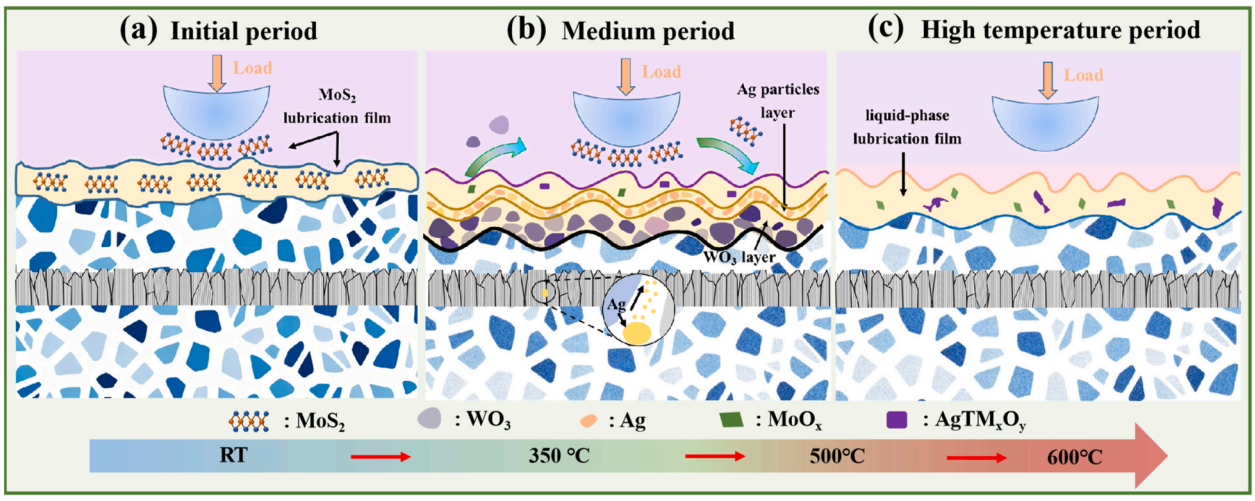

Fig. 10. Elemental diffusion and tribological mechanisms in the continuous heating friction process of S3 coatings at RT-600 °C.

produces trace Mo oxides that coexist with MoS_2 but do not significantly disturb lubrication.

At intermediate temperatures (~500 °C; Fig. 10b), Ag diffusion from the MoAgN base accelerates, although the Mo_2N barrier slows its transport and prevents catastrophic depletion. As the MoS_2-W top layer is gradually consumed, a stratified tribofilm emerges, consisting of a WO_3 base layer, an intermediate Ag-rich layer, and a top layer composed of MoO_3 and $AgTM_xO_y$. Under sliding, the ball initially contacts WO_3 and Ag particles; Ag deforms plastically and spreads, while material produced in earlier low-temperature stages is redistributed and reacts with Ag and Mo oxides to form $AgTM_xO_y$. Simultaneously, WO_3 is transferred to the ball. This dynamic exchange and tribochemical evolution give rise to a self-renewing "sandwich" tribofilm. The intermediate Ag layer functions as a lubricant and a reservoir for continued silver molybdate formation, enabling sustained low friction and moderate wear.

At high temperature (600 °C; Fig. 10c), $AgTM_xO_y$ with low melting points partially melt, coexisting with solid Mo oxides and Ag-Mo-O compounds. The resulting semi-liquid film fills the wear track and adheres to the ball, providing liquid-like lubrication that, together with solid Mo oxides, maintains relatively low COF despite aggressive oxidation. The third-body materials generated during sliding: including compacted oxide layers, silver molybdates, and semi-liquid phases are not merely passive wear products but active participants in lubrication. Their formation, evolution, and eventual ejection determine both the friction coefficient and the net material loss. The Mo_2N diffusion barrier in S3 not only reduces permanent material loss but also promotes the formation of more stable third bodies that remain within the contact zone longer, enhancing lubrication while delaying ejection. This dual function explains the superior wear resistance of S3 despite similar friction coefficients to S2 at some temperatures.

Under high-low temperature cycling, the same sequence of mechanisms is broadly followed. However, repeated exposure to 600 °C, followed by cooling and further sliding at RT, gradually pulverizes the oxide-based tribofilm and suppresses the formation of a coherent transfer film. Once the tribofilm fragments into a loose powder, the system transitions toward dry sliding with high friction and accelerated wear. This comparison underscores that controlling both tribofilm chemistry and mechanical integrity is crucial for achieving durable wide-temperature adaptive lubrication.

4. Conclusions

In this study, we engineered and systematically evaluated three MoAgN-based dual-layer coatings: MoAgN/MoS_2 (S1), MoAgN/MoS_2-W (S2), and MoAgN/MoS_2-W incorporating a columnar Mo_2N diffusion barrier (S3)-deposited by a hybrid HiPIMS-DCMS (High Power Impulse-Direct Current Magnetron Sputtering) process and tested under operando continuous heating (25-600 °C) and high-low temperature cycling. The optimized architecture, S3, delivers the most robust wide-temperature performance: it maintains a friction coefficient below 0.4 across the entire 25-600 °C window and achieves the lowest high-temperature friction (~0.23 at 600 °C), while its wear rate at 600 °C is reduced by a factor of 3.6 relative to the barrier-free MoAgN/MoS_2-W coating. Trace W alloying in the MoS_2 top layer raises the hardness from 4.0 to 5.4 GPa and enhances H/E and H^3/E^2, thereby improving resistance to plastic deformation, cracking, and oxidation without sacrificing lubricity. The columnar Mo_2N interlayer moderates Ag diffusion from the MoAgN base, enabling a controlled Ag supply that prevents rapid depletion and structural weakening. Correlative microstructural and spectroscopic analysis reveals a sequence of temperature-dependent lubrication mechanisms: basal-plane MoS_2 interlayer sliding at low temperature; a self-organized "sandwich" tribofilm at intermediate temperature, comprising a WO_3 base layer, an Ag reservoir, and a MoO_3/$AgTM_xO_y$ top layer; and, at 600 °C, a semi-liquid silver molybdate film coexisting with Mo oxides that sustains low friction under severe oxidation. Under high-low temperature cycling, S3 retains stable, repeatable low friction up to 500 °C through combined MoS_2 shear and oxide-based lubrication, but exposure to 600 °C followed by cooling pulverizes the oxide-based tribofilm into a loose powder, suppresses transfer-film formation, and drives the friction coefficient up to ~0.95, underscoring the importance of tribofilm cohesion in addition to chemical design.

Taken together, these results show that coupling a W-alloyed MoS_2 lubricating top layer with an Ag-containing MoAgN base and an internal Mo_2N diffusion barrier provides an effective materials-architecture strategy for wide-temperature, operando adaptive lubrication. The mechanistic picture established here links controlled noble-metal diffusion, self-organized tribofilm architectures, and their evolution under continuous heating and thermal cycling-offers a general design framework for next-generation adaptive tribological coatings for foil air bearings, high-speed rotating machinery, and other components operating under severe and variable thermal conditions.

CRediT authorship contribution statement

Yong Cheng: Writing – original draft, Investigation, Data curation. **Yupeng Zhang:** Writing – review & editing, Investigation, Formal analysis. **Yingjie Wang:** Methodology. **Yuxi Xu:** Methodology. **Yiqun Feng:** Methodology. **Zhenyu Wang:** Writing – review & editing,

Supervision, Funding acquisition. **Aiying Wang:** Writing – review & editing, Supervision, Funding acquisition, Conceptualization.

Declaration of competing interest

The authors declare that they have no known competing financial interests or personal relationships that could have appeared to influence the work reported in this paper.

Acknowledgements

The work was financially supported by the National Key R&D Program of China (2024YFB3816500), the Natural Science Foundation of Zhejiang Province (LR26E010004), the National Key Research and Development Program of Ningbo (2024Z154, 2025Z135).

Data availability

Data will be made available on request.

References

[1] B. Deng, Y. Tao, X. Zhu, The oxidation behavior and tribological properties of Si-implanted TiN coating, Vacuum 99 (2014) 216.
[2] C. Donnet, A. Erdemir, Historical developments and new trends in tribological and solid lubricant coatings, Surf. Coat. Technol. 180 (2004) 76.
[3] R. Franz, C. Mitterer, Vanadium containing self-adaptive low-friction hard coatings for high-temperature applications: a review, Surf. Coat. Technol. 228 (2013) 1.
[4] H.J. Zhao, L. Yu, C.Y. Mu, Structure and properties of Si-implanted VN coatings prepared by RF magnetron sputtering, Mater. Charact. 117 (2016) 65.
[5] D. Wang, D.S. Su, R. Schlögl, Electron beam induced transformation of MoO_3 to MoO_2 and a new phase MoO, Z. Anorg. Allg. Chem. 630 (2004) 1007–1014.
[6] S. Veprek, M.G.J. Veprek-Heijman, P. Karvankova, Different approaches to superhard coatings and nanocomposites, Thin Solid Films 476 (2005) 1–29.
[7] M.E. Cura, X.W. Liu, U. Kanerva, Friction behavior of alumina/molybdenum composites and formation of MoO_{3-x} phase at 400 °C, Tribol. Int. 87 (2015) 23–31.
[8] G. Gassner, P.H. Mayrhofer, K. Kutschej, Magn'eli phase formation of PVD Mo-N and W-N coatings, Surf. Coat. Technol. 201 (2006) 3335–3341.
[9] I. Asempah, J. Xu, L. Yu, The role of copper incorporation on the microstructure, mechanical and tribological properties of TiBN-Cu films by reactive magnetron sputtering, J. Alloys Compd. 801 (2019) 112–122.
[10] D. Liu, H. Tian, L. Lin, Microstructure, mechanical and elevated temperature tribological behaviors of the diamond/Cu composites prepared by spark plasma sintering method, Diam. Relat. Mater. 91 (2019) 138–143.
[11] H. Guo, M. Han, W. Chen, Microstructure and properties of VN/Ag composite films with various silver content, Vacuum 137 (2017) 97–103.
[12] B. Pavel, J. Peter, M. Hudáková, Cr_2N-7Ag nanocomposite thin films deposited on Vanadis 6 tool steel, Appl. Surf. Sci. 307 (2014) 13–19.
[13] D.V. Shtansky, A.V. Bondarev, V. Kiryukhantsev-Korneevp, Structure and tribological properties of MoCN-Ag coatings in the temperature range of 25-700 °C, Appl. Surf. Sci. 273 (2013) 408–414.
[14] S.M. Aouadi, Y. Paudel, W.J. Simonson, Tribological investigation of adaptive Mo_2N/MoS_2/Ag coatings with highsulfur content, Surf. Coat. Technol. 203 (2009) 1304–1309.
[15] Y.P. Zhang, Z.Y. Wang, S.H. Zhou, Synergistic effect of V and Ag diffusion favored the temperature-adaptive tribological behavior of VAlN/Ag multi-layer coating, Tribol. Int. 192 (2024) 109285.
[16] E. Liu, J. Zhang, S. Chen, High temperature negative wear behaviour of VN/Ag composites induced by expansive oxidation reaction, Ceram. Int. 47 (2021) 15901–15909.
[17] Y.P. Zhang, Z.Y. Wang, Y. Zhang, Self-adaptive lubricating behavior of VAlN/Ag multi-layer coating at simulated operating conditions, J. Mater. Sci. Technol. 229 (2025) 147–158.
[18] X. Xu, J. Sun, F. Su, Microstructure and tribological performance of adaptive MoN-Ag nanocomposite coatings with various Ag contents, Wear (2022) 488–489.
[19] Q.G. Zhang, Y. Zhou, G.J. Zhang, Nanocomposite Mo-Ag-N lubricating, wear resistant and hard coatings fabricated by magnetron sputtering, Mater. Sci. Eng. B 286 (2022) 116066.
[20] B. Deepthi, H.C. Barshilia, K.S. Rajam, Mechanical and tribological properties of sputter deposited nanostructured Cr-WS_2 solid lubricant coatings, Surf. Coat. Technol. 205 (2010) 1937–1946.
[21] J.X. Deng, W.L. Song, H. Zhang, Performance of PVD MoS_2/Zr-coated carbide in cutting processes, Int. J. Mach. Tools Manuf. 48 (2008) 1546–1552.
[22] C. Zeng, J.B. Pu, H.X. Wang, Study on atmospheric tribology performance of MoS_2-W films with self-adaption to temperature, Ceram. Int. 45 (2019) 15834–15842.
[23] Z.X. Lu, C.Z. Zhang, C. Zeng, A novel design by constructing MoS_2/WS_2 multilayer film doped with tantalum toward superior friction performance in multiple environment, J. Mater. Sci. 56 (2021) 17615–17631.
[24] P.G. Grützmacher, M. Schranz, C.J. Hsu, Solid lubricity of WS_2 and Bi_2S_3 coatings deposited by plasma spraying and air spraying, Surf. Coat. Technol. 446 (2022) 128772.
[25] X.Y. Ma, Q. Gao, Z.R. Gao, Oxygen-induced contact evolution enables friction reduction in MoS_2/Ag composite films, Friction 13 (2025) 9441108.
[26] K. Holmberg, A. Matthews, Coatings Tribology: Properties, Mechanisms Techniques and Applications in Surface Engineering, Elsevier Science, Netherland, 2009.
[27] L. Zhang, X.J. Liao, R. Chen, Tribological behavior of NiAl coating deposited by plasma spraying of diamond-contained Ni/Al composite powder at a wide range temperature from 25 °C to 700 °C, Transactions of Materials Research 1 (2025) 100100.
[28] X.H. Zhou, Y.P. Zhang, H. Li, Cr doping modification for tribological behavior of Cr/a-C multilayer coatings against PEEK under diverse operational conditions, Friction 13 (2025) 9440920.
[29] L. Li, Z.X. Lu, J.B. Pu, Investigating the tribological and corrosive properties of MoSui/Zr coatings with the continuous evolution of structure for high-humidity application, Appl. Surf. Sci. 541 (2021) 148453.
[30] M. Gardos, The synergistic effects of graphite on the friction and wear of MoS_2 films in air, ASLE Trans 31 (1988) 214–227.
[31] K.F. Koo, G.L. Schrader, Method for Preparing Basal Oriented Molybdenum Disulfide (MoS_2) Thin Films, Google Patents, 1994.
[32] Z.Y. Wang, X.W. Li, X. Wang, Hard yet tough V-Al-C-N nanocomposite coatings: microstructure, mechanical and tribological properties, Surf. Coat. Technol. 304 (2016) 553–559.
[33] X.Y. Liu, X.H. Pei, H.M. Wang, Unlocking metallic glasses ultra-low friction via high-entropy effect and oxidation, Int. J. Mech. Sci. 301 (2025) 110507.
[34] C.C. Tang, M. Steinbrueck, M. Stueber, Deposition, characterization and high-temperature steam oxidation behavior of single-phase Ti_2AlC-coated Zircaloy-4, Corros. Sci. 135 (2018) 87–98.
[35] H. Singh, K.C. Mutyala, R.D. Evans, An investigation of material and tribological properties of Sb_2O_3/Au-doped MoS_2 solid lubricant films under sliding and rolling contact in different environments, Surf. Coat. Technol. 284 (2015) 281–289.
[36] B. Chakraborty, H.S.S.R. Matte, A.K. Sood, Layer-dependent resonant Raman scattering of a few layer MoS_2, J. Raman Spectrosc. 44 (2013) 92–96.
[37] D. Stone, J. Liu, D.P. Singh, Layered atomic structures of double oxides for low shear strength at high temperatures, Scripta Mater. 62 (2010) 735–738.
[38] E. Liu, J. Zhang, S. Chen, High temperature negative wear behaviour of VN/Ag composites induced by expansive oxidation reaction, Ceram. Int. 47 (2021) 15901–15909.
[39] R. Tyagi, D.S. Xiong, J.L. Li, Elevated temperature tribological behavior of Ni based composites containing nano-silver and hBN, Wear 269 (2010) 884–890.
[40] W. Gulbinski, T. Suszko, Thin films of MoO_3-Ag_2O binary oxides-the high temperature lubricants, Wear 261 (2006) 867–873.
[41] E. Laolu-Balogun, S. Owen, S. Read, Effect of humidity and oxygen on friction, wear and durability of a polymer-bonded molybdenum disulfide (MoS_2)-based dry film lubricant (DFL) coating system in large amplitude fretting, Wear 552–553 (2024) 205426.
[42] Z.R. Gao, W.M. Nie, H.X. Wang, Enhancing mechanical performance and high-temperature lubrication enabled by MoS_2/WB_2 nanolayered films, Composites, Part B 275 (2024) 111350.
[43] J.H. Hsieh, C.H. Chiu, C. Li, Development of anti-wear and anti-bacteria TaN-(Ag, Cu) thin films-A review, Surf. Coat. Technol. 233 (2013) 159–168.
[44] C.P. Mulligan, T.A. Blanchet, D. Gall, CrN-Ag nanocomposite coatings: High-temperature tribological response, Wear 269 (2010) 125–131.
[45] B. Pavel, J. Peter, M. Hudáková, Cr_2N-7Ag nanocomposite thin films deposited on Vanadis 6 tool steel, Appl. Surf. Sci. 307 (2014) 13–19.
[46] C.P. Mulligan, P.A. Papi, D. Gall, Ag transport in CrN-Ag nanocomposite coatings, Thin Solid Films 520 (2012) 6774–6779.